Theory of the Frenkel–Debye boundary layer at the (111) surface of pure CaF_2

2003 J. Phys.: Condens. Matter 15 5801

(http://iopscience.iop.org/0953-8984/15/34/310)

INSTITUTE OF PHYSICS PUBLISHING JOURNAL OF PHYSICS: CONDENSED MATTER

J. Phys.: Condens. Matter **15** (2003) 5801–5820 PII: S0953-8984(03)61069-6

Theory of the Frenkel–Debye boundary layer at the (111) surface of pure CaF_2

Heinz Dabringhaus[1,3] **and Mikhail F Butman**[2]

[1] Mineralogisch-Petrologisches Institut, Universität Bonn, Poppelsdorfer Schloss, D-53115 Bonn, Germany
[2] Department of Physics, State University of Chemical Sciences and Technology, Prospekt Engelsa 7, 153460 Ivanovo, Russia

E-mail: h.dabringhaus@uni-bonn.de

Received 13 March 2003, in final form 16 July 2003
Published 15 August 2003
Online at stacks.iop.org/JPhysCM/15/5801

Abstract

The present paper is concerned with a theoretical study of the properties of the Frenkel–Debye boundary layer at the (111) surface of pure (undoped) CaF_2, a crystal with anti-Frenkel defects, i.e. with anion vacancies and interstitials. The study is based on theoretical determinations of the adsorption energies of the fluorine ion at the terrace, step and kink sites on the surface, which are, together with the assumption of experimental step distances and theoretical kink concentrations, necessary pre-requisites for a quantitative description of the surface charge compensating that of the space-charge region. The results show that, for realistic surface conditions, the surface and space charges, and with them the potential between surface and bulk, are reduced considerably compared with those for an unlimited number of accessible surface sites. Nevertheless, on approaching the surface a strong increase in the anion vacancy concentration against that of the bulk still exists, which should lead to an increased ion conductivity in near-surface regions and thin fluorite layers.

1. Introduction

It was first pointed out by Frenkel [1] and later, independently, by Lehovec [2] that near the surface of ionic crystals a space-charge region exists, this charge being compensated by a charge of opposite sign on the surface. Because the lateral extension of this electric dipole layer is of the order of a Debye length this layer is denoted as the Frenkel–Debye (FD) layer. Its origin, fundamentally, can be ascribed to differences in the free energies of formation of point defects such as cation and anion vacancies in the case of Schottky disorder and as vacancies

[3] Author to whom any correspondence should be addressed.

and interstitials for Frenkel disorder. While in the bulk of the crystal, due to the condition of electrical neutrality, the charges of the different point defects must cancel out, in the immediate proximity of the surface their mole fractions adjust independently from each other with respect to their individual free formation energies. Connected with the FD layer is an electrical field perpendicular to the surface, which ensures a smooth transition between the near-surface and bulk mole fractions of the defects.

Later on, the theory of the FD layer was refined and extended to the case of divalent cation additives in NaCl-type crystals with Schottky disorder by Kliewer and Koehler [3]. The effect of a segregation of the impurities at the surface was considered by Blakely and Danyluk [4]. Kliewer and Koehler [3] and Margvelashvili and Saralidze [5] calculated the properties of thin layers, i.e. of crystals with a limited thickness in one dimension and infinite extensions in the other two, in which the electric potential is reduced due to the overlap of the space-charge clouds at both surfaces. Kliewer [6] applied the theory to the case of Frenkel disorder. Eshelby *et al* [7] showed that space-charge regions should exist also around inner surfaces, i.e. the cores of dislocations, of ionic crystals. Poeppel and Blakely [8] pointed to the fact that the energies involved in the creation of the point defects are not unique properties of the crystal bulk but depend specifically on the features of the surface. Among others, the finite number of surface sites, at which the excess ions on the surface are adsorbed, must be taken into account. This effect should lead to a strong reduction of the space-charge potential, especially at higher temperatures, so that the results of Lehovec [2] and Kliewer and Koehler [3] represent limiting cases only.

Although the theory of the FD layer has been studied under a variety of aspects, as far as is known to the present authors, until now no attempts have been made to base it on realistic features of the surface, i.e. on concrete values of the binding energies of the excess ions at the different surface sites, kinks, steps and terraces, as well as on actual, i.e. experimentally available, densities of these sites. In a series of studies we currently investigate the growth and evaporation of CaF_2 crystals [9–11]. CaF_2 is, as the most prominent representative of crystals with the fluorite structure, not only of basic scientific interest, but also a material of great technological importance. This concerns, for example, bulk growth of large CaF_2 crystals for nano-lithography, see, e.g., [12], as well as the formation of thin epitaxial layers on semiconductors: above all, because of the low misfit on silicon [13, 14]. Within our studies we have recently also carried out theoretical determinations of the adsorption energies of the CaF_2 molecule at different sites on the (111) surface of the CaF_2 crystal [15] as well as of diffusion pathways on the terrace [16]. CaF_2 is known to possess anti-Frenkel disorder [17], which means that fluorine ions are removed from their normal lattice positions into interstitial sites located in the vacant cubes of the cubic primitive fluorine sublattice, i.e. in those ones which are not occupied by calcium ions. It suggests we extend our theoretical calculations to the case of the adsorption of the F^- ion at the different surface sites and to lay in this way the base for a realistic determination of the features of the FD layer for this important type of crystal.

In the following we will at first develop the theory of the FD layer for a fluorite-type crystal with anti-Frenkel defects in thermodynamic equilibrium. We will then focus on results of the calculations of the adsorption energies of fluorine ions on the (111) surface of CaF_2 and finally give a description of the properties of the FD surface layer at the (111) surface of a pure CaF_2 crystal under consideration of experimentally accessible step distances at the surface. Additionally, the present studies, because of their importance for the ion conductivity of nano-crystalline CaF_2 material [18] as well as for the case of epitaxial layers, for example, on semiconductors (see above), will be extended to the case of thin CaF_2 layers with free (111) surfaces.

2. Theory of the Frenkel–Debye boundary layer for a fluorite-type crystal

2.1. Semi-infinite crystal

In a fluorite-type crystal with anti-Frenkel disorder anions can be removed from their normal lattice sites and put into interstitial sites as well as adsorbed at specific sites on the surface. As such surface adsorption sites the positions at kinks, steps and terraces come into question. The semi-infinite crystal under consideration extends from $x = 0$ (surface) to $x = \infty$ and from $-\infty$ to ∞ in the y and z directions. The total Gibbs free energy of this disordered crystal may be expressed as

$$\begin{aligned} G = G_0 + \int_0^\infty \Bigg\{ & n_i(x) F_f + \tfrac{1}{2}\rho(x)\Phi(x) \\ & - kT \ln \frac{(2N_b)!}{[2N_b - n_v(x)]!\, n_v(x)!} - kT \ln \frac{N_b!}{[N_b - n_i(x)]!\, n_i(x)!} \Bigg\} \mathrm{d}x \\ & + n_k F_k + n_l F_l + n_t F_t - kT \ln \frac{N_k!}{(N_k - n_k)!\, n_k!} \\ & - kT \ln \frac{N_l!}{(N_l - n_l)!\, n_l!} - kT \ln \frac{N_t!}{(N_t - n_t)!\, n_t!}, \end{aligned} \tag{1}$$

where the first term, G_0, on the right side of equation (1) gives the energy of the perfect crystal, the integral term describes the Gibbs free energy of the FD layer and the remaining terms represent the contributions of the surface. Here, N_b is the number of molecular units per volume unit. While the number of accessible interstitial sites is equal to N_b, the number of regular anion sites corresponds to $2N_b$. N_k, N_l and N_t are the available kink, step (= ledge) and terrace sites on the surface per unit of area. The actual concentrations of the anion vacancies and interstitials in the bulk are represented by n_v and n_i, respectively, and those of the anions at kink, step and terrace sites on the surface by n_k, n_l and n_t. The free energy for creating a Frenkel defect, i.e. for taking an anion from a normal bulk site into an interstitial site, is denoted as F_f. The free energies for moving anions from normal bulk sites to kink, step and terrace sites are F_k, F_l and F_t, respectively. $\Phi(x)$ denotes the potential in the FD layer and $\rho(x)$ the space-charge density.

For charge neutrality of the crystal the space-charge in the FD layer

$$\int_0^\infty \rho(x)\,\mathrm{d}x = \int_0^\infty e\,[n_v(x) - n_i(x)]\,\mathrm{d}x, \tag{2}$$

where e is the elementary charge, must be compensated by a surface charge

$$\sigma = -e\,(n_k + n_l + n_t) \tag{3}$$

of opposite, here always negative, sign (compare section 3.2), i.e.

$$n_k + n_l + n_t - \int_0^\infty [n_v(x) - n_i(x)]\,\mathrm{d}x = 0. \tag{4}$$

In the above equations, as usual, a positive elementary charge is assigned to the anion vacancy, while all other species carry negative elementary charges. The potential in the space-charge region is connected with the vacancy and interstitial concentrations by Poisson's equation:

$$\frac{\mathrm{d}^2\Phi(x)}{\mathrm{d}x^2} = -\frac{4\pi}{\epsilon}\rho(x) = \frac{4\pi e}{\epsilon}[n_i(x) - n_v(x)], \tag{5}$$

where ϵ is the static dielectricity constant.

The minimization of the Gibbs free energy given in equation (1) and the solution of the electrostatic problem connected with it are described in appendix A. Finally, an equation for

the potential difference between surface and bulk, Φ_∞, is achieved, which may be solved numerically:

$$\left(\frac{\sqrt{2}N_b\epsilon kT}{\pi e^2}\right)^{1/2}\exp\left(-\frac{F_f}{4kT}\right)\sinh\left(\frac{e\Phi_\infty}{2kT}\right)=N_k\left[\sqrt{2}+\exp\left(\frac{F_k-F_f/2+e\Phi_\infty}{kT}\right)\right]^{-1}+N_l\left[\sqrt{2}+\exp\left(\frac{F_l-F_f/2+e\Phi_\infty}{kT}\right)\right]^{-1}+N_t\left[\sqrt{2}+\exp\left(\frac{F_t-F_f/2+e\Phi_\infty}{kT}\right)\right]^{-1}. \tag{6}$$

With a knowledge of Φ_∞, from equation (A.19) in appendix A, using (A.12) and (A.13), the course of the potential $\Phi(x)$ in the space-charge layer, and with this the dependence of the vacancy and interstitial concentrations on the distance from the surface, x, as well as the respective surface concentrations, can be calculated:

$$\begin{aligned}
n_v(x)&=\sqrt{2}\,N_b\exp\left(-\frac{F_f/2+e\Phi(x)-e\Phi_\infty}{kT}\right)\\
n_i(x)&=\sqrt{2}\,N_b\exp\left(-\frac{F_f/2-e\Phi(x)+e\Phi_\infty}{kT}\right)\\
n_k&=N_k\left\{1+\frac{1}{\sqrt{2}}\exp\left(\frac{F_k-F_f/2+e\Phi_\infty}{kT}\right)\right\}^{-1}\\
n_l&=N_l\left\{1+\frac{1}{\sqrt{2}}\exp\left(\frac{F_l-F_f/2+e\Phi_\infty}{kT}\right)\right\}^{-1}\\
n_t&=N_t\left\{1+\frac{1}{\sqrt{2}}\exp\left(\frac{F_t-F_f/2+e\Phi_\infty}{kT}\right)\right\}^{-1}.
\end{aligned} \tag{7}$$

2.2. Thin crystal layer

In the present section the above derivation for a semi-infinite crystal is extended to the case of a thin layer of a fluorite-type crystal. The layer, width in x direction $= 2L$, should have free (111) surfaces at $x = 0$ and $2L$. The extension in the y and z directions is assumed to be infinite. Here, the potential has an extremum at the middle plane, $x = L$, and the boundary condition (A.16) must be replaced by

$$\mathrm{d}\Phi(x)/\mathrm{d}x|_L = 0. \tag{8}$$

The treatment of this problem (see appendix B) leads to an equation which connects the potential Φ_L at the middle plane of the layer with the parameter $e\tilde{\Phi}_\infty$:

$$\left(\frac{N_b\epsilon kT}{\sqrt{2}\pi e^2}\right)^{1/2}\exp\left(-\frac{F_f}{4kT}\right)\left\{\cosh\left(\frac{e\tilde{\Phi}_\infty}{kT}\right)-\cosh\left(\frac{e\tilde{\Phi}_\infty-e\Phi_L}{kT}\right)\right\}^{1/2}=-\left\{N_k\left[\sqrt{2}+\exp\left(\frac{F_k-F_f/2+e\tilde{\Phi}_\infty}{kT}\right)\right]^{-1}+N_l\left[\sqrt{2}+\exp\left(\frac{F_l-F_f/2+e\tilde{\Phi}_\infty}{kT}\right)\right]^{-1}+N_t\left[\sqrt{2}+\exp\left(\frac{F_t-F_f/2+e\tilde{\Phi}_\infty}{kT}\right)\right]^{-1}\right\}. \tag{9}$$

With the knowledge of this dependence equation (B.3) can be evaluated, which yields the dependence of the potential in the layer, $\Phi(x)$, on the distance from the surface, x, and

with it also the vacancy and the interstitial concentrations as a function of x. The surface concentrations could be already calculated with $\tilde{\Phi}_\infty$ using equation (7) correspondingly.

3. The adsorption of fluorine ions at the (111) surface of CaF_2

3.1. Characterization of the (111) surface of CaF_2

The application of the above theory to a specific crystal surface, here the (111) surface of CaF_2, demands a knowledge of its properties, above all of the densities of step and kink sites as well as of the determination of the energies for the adsorption of the excess surface anions in the respective surface sites.

The CaF_2 structure (space-group: $Fm\bar{3}m$; lattice constant $a_0 = 0.5463$ nm [19], number of molecules per cm^{-3}: $N_b = 2.457 \times 10^{22}$) may be considered as a sequence of F^-–Ca^{2+}–F^- triple layers stacking in the [111] direction. In the bulk of the crystal the spacing of these triple layers amounts to $a_0/\sqrt{3} = 0.3154$ nm and the distance of the upper and lower fluorine layer to the intermediate calcium layer to $a_0/(4\sqrt{3}) = 0.0789$ nm. (111) is the cleavage face of CaF_2. It is, however, also the growth face under clean, i.e. vacuum, conditions [10]. The relaxation of the (111) surface is small. It concerns essentially the outermost surface triple layer. Values for the surface relaxation are given in [20]. The relaxation of the outermost surface layer has the effect that the potential above the surface, at a distance, in which the influences of the individual surface ions cancel out each other, adopts a constant value of $\Phi_{out} = +0.354$ V, instead of a vanishing potential for an unrelaxed surface.

The number of terrace sites, at which a fluorine ion can adsorb (see section 3.2), equals the number of calcium sites, which amounts to

$$N_t = 4(\sqrt{3}\,a_0^2)^{-1} = 7.74 \times 10^{14}\ \mathrm{cm}^{-2}. \tag{10}$$

Since the experimental step distance is usually large relative to the smallest possible step distance of $\sqrt{3/8}\,a_0$, the number of terrace sites is only negligibly decreased by the presence of steps.

Steps on the thermally activated (111) surface run in the ⟨110⟩ directions [9]. These steps are of the so-called I type [9]. They can be regarded as small {110} mini-facets. Relaxations of the ions at the ⟨110⟩-I step are again small. Values for the coordinates of the relaxed step ions can also be taken from [20]. The step distance depends on the pre-treatment of the surface and the temperature. On cleaved surfaces, the steps, which usually have a height of one triple layer, run predominantly in the ⟨110⟩ and ⟨211⟩ directions. Step distances were determined to be between 40 and 80 nm [9]. The step distance varies further with the specific location on the surface. It depends, above all, on the local dislocation density. Cleavage topographies are maintained up to temperatures of about 820 K. Above this temperature the cleavage topography changes into a topography with almost triangular islands [9]. Here, only ⟨110⟩ steps of the type I are found. An increase of the temperature up to 1050 K leads to a progressive flattening of the surface, with step distances increasing from 20 to 100 nm. Above 1050 K at a free surface, evaporation starts, which leads again to a decrease of the step distances. For surfaces grown at a temperature of 1055 K and a saturation ratio of 354, ⟨110⟩-I steps were found to be arranged in growth hills with closed step lamella [11]. Here the step distance amounted to about 60 nm. Summarizing these different results, one comes to the conclusion that the step distances on the $CaF_2(111)$ surface at experimentally accessible conditions should lie in the range $\lambda = 10$–100 nm, corresponding to densities of step sites of

$$N_l = \sqrt{2}/(a_0\lambda) = 2.6 \times 10^{13} - 2.6 \times 10^{12}\ \mathrm{cm}^{-2}. \tag{11}$$

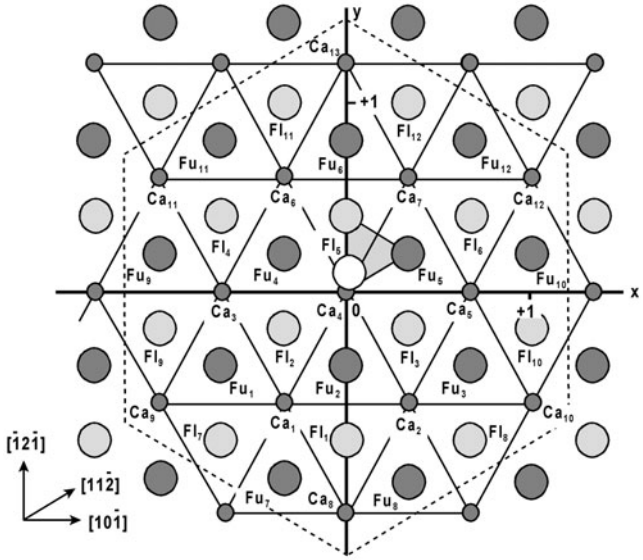

Figure 1. Schematic outline of the first triple layer of the (111) surface of CaF_2 in a top view. Small grey circles, Ca^{2+} ions; large grey circles, ions Fu of the upper fluorine layer; large hatched circles, ions Fl of the lower fluorine layer of the first TL. Ions of the chosen terrace adregion are enclosed by the broken line. The fluorine adion is indicated as a large white circle. From symmetry reasons for the adion only those positions above the grey marked triangle need to be considered.

The configuration of the kink at a ⟨110⟩-I step was determined in [15]. The formation energy resulted as $E_f^k = 0.47$ eV. With this the temperature dependence of the kink density on the (111) surface can be described as

$$N_k = 2N_l \exp(-E_f^k/kT) = 2N_l \exp(-5.487 \times 10^3/T)\ \mathrm{cm}^{-2}. \tag{12}$$

3.2. Determination of adsorption positions and energies

The FD theory starts with the assumption that an excess number of ions of one kind is adsorbed on the surface. In the case of a calcium fluoride crystal this concerns the fluorine ion. For $CaF_2(111)$ values of the adsorption energies of the fluorine adion, F_{ad}^-, at the different surface sites (terrace, step and kink) are not known until now. We have therefore performed corresponding calculations subsequently to calculations of adsorption energies of the CaF_2 molecule at these positions [15]. An important factor in such calculations is the consideration of additional relaxations of ions of the crystal due to interactions with the adsorbed ion. Since these relaxations concern, in essence, ions in the vicinity of the adsorbed ion, so-called adsorption regions, in brief: adregions, around the adion were defined, in which the ions of the crystal were allowed to adjust their positions to new minimum values of the total potential energy. As an example, figure 1 (compare also table 1) shows the adregion defined for the calculation of the adsorption on the terrace. This adregion comprises 12 ions of the upper fluorine layer (Fu_1–Fu_{12}), 12 ions of the lower fluorine layer (Fl_1–Fl_{12}) and 13 ions of the intermediate calcium layer (Ca_1–Ca_{13}), in all 37 ions of the uppermost triple layer of the crystal. By varying the sizes of the adregions it was shown that the chosen extensions (see table 2) were sufficient to calculate the relaxation energies to an overall accuracy of about 3%. Ions of the second triple layer, i.e. the layer below the topmost TL, were not considered in the

Table 1. Position of the F^- adion at the terrace of $CaF_2(111)$ as well as initial and final (x, y, z) positions (compare figure 1) of the ions of the adregion, first and second lines, respectively. The r are distances of the ions of the adregion from the adion in the final position, with Δr their total displacements. Coordinates are given as normalized values with respect to the lattice constant a_0. Ions which are symmetrical to the listed ones with the same r and Δr values are given in parentheses. Ions which are only nearly symmetrical (because of the non-central symmetry of the adregion) are given in brackets.

	x	y	z	r	Δr
F_{ad}	0.0	−0.0003	0.4430		
Ca_4	0.0	0.0	−0.0033		
	0.0	−0.0002	0.0647	0.3783	0.0680
Ca_1 (Ca_2) [Ca_3, Ca_5–Ca_7]	−0.3536	−0.6124	−0.0033		
	−0.3510	−0.6076	−0.0016	0.8305	0.0056
Ca_8 [Ca_9–Ca_{13}]	0.0	−1.2247	−0.0033		
	0.0	−1.2186	−0.0019	1.2970	0.0063
Fu_2 [Fu_4, Fu_5]	0.0	−0.4082	0.1302		
	0.0002	−0.4364	0.1114	0.5478	0.0339
Fu_1 (Fu_3) [Fu_6]	−0.7071	−0.4082	0.1302		
	−0.7182	−0.4150	0.1309	0.8862	0.0130
Fu_7 (Fu_8) [Fu_9–Fu_{12}]	−0.3536	−1.0206	0.1302		
	−0.3571	−1.0261	0.1341	1.1293	0.0076
Fl_2 (Fl_3) [Fl_5]	−0.3536	−0.2041	−0.1461		
	−0.3661	−0.2115	−0.1441	0.7235	0.0147
Fl_1 [Fl_4, Fl_6]	0.0	−0.8165	−0.1461		
	0.0	−0.8321	−0.1555	1.0247	0.0182
Fl_7 (Fl_8) [Fl_9–Fl_{12}]	−0.7071	−0.8165	−0.1461		
	−0.7074	−0.8212	−0.1491	1.2349	0.0056

Table 2. Adsorption energies E_{ad} (eV) of a fluor ion at the terrace (T), step (L) and kink (K) positions on the $CaF_2(111)$ surface. N_{ad}: number of ions in the adregion; E_{int}: interaction energy of the F^- adion with the crystal; E_{reg}^{rel}: relaxation energy of the adregion; E_{ad}: total adsorption energy.

	N_{ad}	E_{int}	E_{reg}^{rel}	E_{ad}
T	38	−3.939	1.349	−2.590
L	36	−4.396	0.773	−3.623
K	32	−6.247	1.896	−4.351

adregions because their relaxations will be small. This is caused, on the one hand, by the small relaxations of the fluorine ions Fl of the topmost TL (see table 1). Further, each triple layer, as an F^-–Ca^{2+}–F^- layer sequence, is itself energetically saturated to some extent. It should be noted, in addition, that in the present calculations, as in the earlier determinations of the adsorption of the CaF_2 molecule [15], no periodic boundary conditions were used, because this may lead to errors in the Coulomb energy. This will be true all the more for a charged cell as in the present case.

Calculations of the total interaction energies were based on the Coulomb and a nearest-neighbour interaction potential:

$$V_{ab}(r) = \frac{q_a q_b}{r} + A_{ab}\exp\left(-\frac{r}{\rho_{ab}}\right) - \frac{C_{ab}}{r^6}. \tag{13}$$

Here, r is the distance between ions a and b, which have the charges q_a and q_b, and A, ρ and C are parameters [21], compare also [15]. Virtually the same potential was applied by

Dornford-Smith and Grimes to study vaporization mechanisms of CaF_2 nano-crystallites [22]. These authors showed that with this potential for the free molecule as well as for the CaF_2 crystal results are obtained which are in good correspondence to quantum mechanical calculations. In [9] we showed that with the above potential experimental features of the free CaF_2 molecule can be well reproduced. Special ionic polarization according to a shell model [23] was not considered in our calculations. Owing to the large calculational complexity this is, however, often done in static calculations of this kind (compare [22]). A subsequent determination of the induced dipole moment of the fluorine in its equilibrium adsorption position on the terrace showed that the electrical energy associated with it can indeed be neglected against the other terms, especially the energy resulting from the relaxation of ions of the adregion.

The Coulomb energy was calculated for a thin slab, comprising four triple layers of infinite extension parallel to the surface. This slab was thick enough to achieve an accuracy of 10^{-5} eV. The calculations were started with completely relaxed terrace, step and kink sites without adsorption ('crystal relaxed' positions). The fluorine ion was initially positioned above a calcium ion of the uppermost triple layer close to the centre of the respective adregion. The adion, as well as the ions of the adregion, were allowed to relax their positions under the action of the potential modified by the adion as well as by additional displacements of the ions of the adregion. In particular the Coulomb interaction between the adion and the ions of the adregion and of these ions with the remaining crystal was calculated

(i) by an Ewald summation over the CaF_2 slab [24, 25] with all ions being in their initial 'crystal relaxed' positions,
(ii) subtracting from this the interactions with the ions of the adregion in these positions, and
(iii) adding the corresponding interactions where the ions are in their modified 'adion relaxed' positions.

For asymmetrical regions, i.e. half-planes and half-steps beside the step and the kink, where an Ewald summation is not possible, a direct summation over corresponding crystal regions was performed. The final equilibrium adsorption positions were determined by varying the coordinates of the adsorbed F^- ion and of the ions of the chosen adregion until a minimum of the total energy of the system was obtained. More details about the calculational procedure can be found in [15] and [20].

For the terrace case, the starting and final coordinates of the adion and of the ions of the adregion, as well as the total spatial displacements, are compiled in table 1. For the step and kink cases, corresponding coordinate values may be requested from the authors. In table 1 (compare also figure 1), the coordinates are given as normalized values, where one unit corresponds to the lattice constant a_0 of CaF_2. It is seen that the relaxations concern essentially ions in the immediate vicinity of the adion. They amount to maximal values of about 0.07 length units (0.4 Å) and decrease strongly with increasing distance from the adion.

Figure 2 comprises the resulting positions of the F^-_{ad} ion for the adsorption at the terrace (T), step (L) and kink (K) sites. It is seen that in the terrace and kink positions the fluorine adion is located above calcium ions of the outermost triple layer while at the step it is adsorbed above a calcium in the [110] direction of the (110) mini-facet. In the terrace and kink cases these positions correspond, in essence, to the usual continuation of the lattice in the [111] direction. In the step case the adsorption position is determined mainly by the especially strong interaction energy with the underlying calcium ion (compare [15]). A virtual slight shift in the direction towards the upper terrace would, however, also result in a position corresponding to a lattice continuation in the [111] direction. At the kink the adsorbed fluorine ion fills up a position at the end of the lower fluorine row of the mini-facet. In this way, the initially electrical neutral kink [15] is transformed into a negatively charged one.

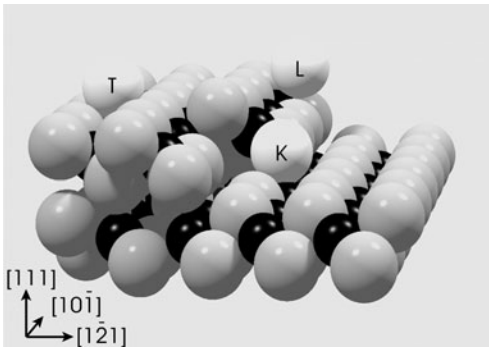

Figure 2. Adsorption positions of a fluor adion (white) at the terrace (T), the [10$\bar{1}$]-type I step (L) and the kink at the [10$\bar{1}$]-type I step (K) on the $CaF_2(111)$ surface; calcium ions: black, fluorine ions: grey.

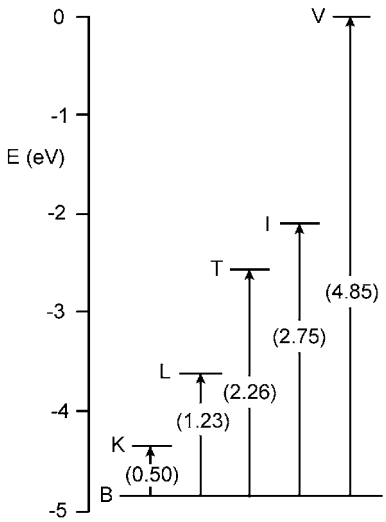

Figure 3. Energy term scheme for a fluorine ion in bulk (B), interstitial (I), kink (K), step (L) and terrace (T) positions with respect to the vacuum level (V) at 0 eV. The numbers in parentheses indicate the energy differences at the above positions relative to the bulk state.

The adsorption energies, E_{ad}, in the above positions (table 2) are made up of two contributions. The first term is the interaction energy, E_{int}, of the adion with the additionally relaxed terrace, step and kink environment and the remaining crystal and the second one the relaxation energy of the adregion, E_{reg}^{rel}. This latter term is always positive, because it represents the difference in energies of the adregion (or the crystal) in the final state with adsorption and its initial 'crystal relaxed' state without adsorption. As expected, the adsorption energy increases from the terrace over the step to the kink position. The relatively low value of the relaxation energy of the adregion for adsorption at the step of 0.77 eV is remarkable. This is an indication of the strong bonding of the ions of this (110) mini-facet, and hence of the stability of this step configuration.

The different bulk and surface energy levels for a F^- ion, which are of interest in the present connection, are compiled in figure 3 with respect to a vacuum level. As was mentioned in the preceding section, the potential above the relaxed infinite (111) surface of CaF_2 without

adsorption amounts to +0.35 V, so that, with respect to this level, all desorption energies at the surface should be reduced correspondingly. In the present case, however, surface and bulk values, for convenience, are referred to a uniform vacuum level at 0 V. Moreover, for a calculation of the FD space-charge layer at $CaF_2(111)$, only the energy differences of the adsorption sites to the normal bulk lattice site at -4.85 eV below the vacuum level [21] are of importance. These differences are indicated by arrows in figure 3, while corresponding numerical values are given in parentheses.

4. The Frenkel–Debye layer for $CaF_2(111)$

4.1. Semi-infinite crystal

With the above values for the first time concrete properties of the FD layer for an ionic crystal, here for the (111) surface of CaF_2 ($\epsilon = 6.79$ [26]), will be characterized. Defect energies in the bulk of CaF_2 were determined theoretically by Catlow *et al* [21]. For the formation energy of anion vacancies, i.e. for the energy to remove a fluorine ion from its normal lattice position to infinity leaving a vacancy, they obtained a value of 4.85 eV and for the energy to introduce a fluorine from infinity into an interstitial lattice site a value of -2.10 eV. With this, the formation energy of an anion Frenkel pair results as the sum of both energies to 2.75 eV. The energies to bring a calcium ion from a lattice site to infinity as well as to an interstitial position are, at 23.17 and 8.0 eV [21], respectively, quite large. Additionally our own calculations of the adsorption energies of the Ca^{2+} ion at the different surface sites yield the following values: -5.48 eV at the terrace, -6.97 eV at the step, -7.13 eV at a neutral kink and -14.32 eV at a negatively charged kink, i.e. at a kink with adsorbed fluorine, compare figure 2. For the transition of a cation from the bulk to the surface, therefore, at least an energy of 8.9 eV is needed, which shows that the concentrations of cation vacancies are low. They can, therefore, be neglected in the present discussion.

The results of the calculations for the FD layer under consideration of fluorine ions in different surface, as well as in interstitial, positions are comprised of the following. The temperature dependence of the Debye length, which depends not on the specific surface features but only on the formation energy of the Frenkel pair (see equation (A.14)) results in

$$\kappa^{-1} = 6.82 \times 10^{-11}\sqrt{T}\exp(7978/T)\ \text{cm}. \tag{14}$$

This value is a measure of the extension of the space-charge region into the crystal. It amounts to about 10^{-5} cm at 1000 K and to about 1 cm at 400 K. At room temperature κ^{-1} reaches a value of about 10 m. For such low temperatures the results for the thin layer must be used. However, apart from the fact that at low T thermodynamical equilibrium will hardly be achieved within experimental times because the diffusion processes will be more or less frozen, here the defect concentrations should be dominated by impurity effects.

Figures 4–6 show the potential differences between bulk and surface of the semi-infinite crystal as well as the concentrations of the fluorine adions at the kinks and steps as a function of the temperature with the step distance λ as a parameter. Terrace concentrations are not given because their values are lower by a factor of, at least, 10^4 than those at the kinks and steps. The experimentally accessible range of $10^{-6} < \lambda < 10^{-5}$ cm is shaded in the figures. The potential in the bulk (figure 4) is always positive with respect to the surface. Its value in the experimentally accessible range lies between 0.23 and 0.53 V for temperatures between 400 and 1400 K. It is considerably lower than that for a completely roughened surface with $\lambda = 10^{-8}$ cm. In figure 5, beside the adion concentration at the kinks n_k (full lines) the total density of kinks N_k (broken lines) in dependence on the temperature and the step distance is

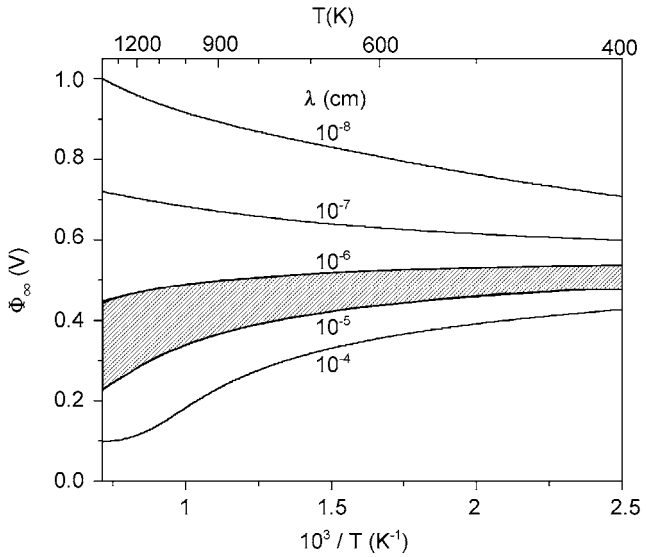

Figure 4. The potential difference Φ_∞ between bulk and surface as a function of temperature for different step distances λ as a parameter. The region of experimentally accessible step distances is shaded.

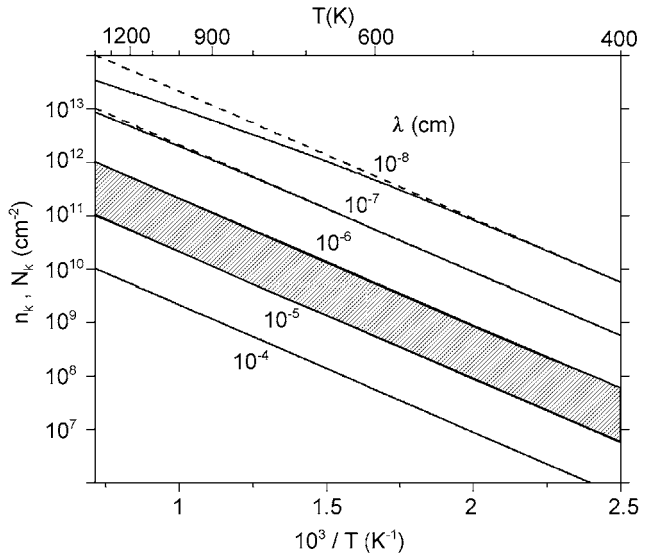

Figure 5. The density of fluorine ions n_k in the kinks (full lines) and the total density of the kinks N_k (broken lines) as a function of temperature.

also given. The comparison of both quantities shows that, for $\lambda \geqslant 10^{-7}$, practically all kinks are occupied by an additional fluorine ion, i.e. all neutral kinks become negatively charged ones. This is surprising, because in a recent calculation of the kink configuration it turned out that the neutral kink had the lowest formation energy [9]. In those calculations, however, only surface properties were included. For constant temperature the concentration of fluorine adions in the kink sites (or that of negatively charged kinks) increases almost inversely proportional to

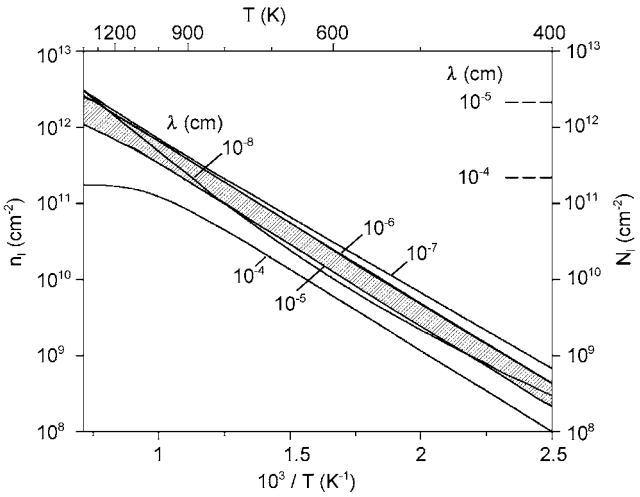

Figure 6. The density of fluorine ions n_I at the steps (full lines) as a function of temperature. On the right axis total densities of step sites are indicated as broken lines.

the step distance. In the experimentally accessible range its concentration increases from about 5×10^7 at 400 K to about $5 \times 10^{11}/\mathrm{cm}^{-2}$ at 1400 K. The concentration of adions at the steps (figure 6) shows a corresponding increase from 3×10^8 to $2 \times 10^{12}/\mathrm{cm}^{-2}$ in the same range. A comparison with the total density of step sites N_I (broken lines indicated on the right axis in figure 6) shows that the capacity of the steps for the adion accumulation is usually far from being exhausted. Only for large step distances of 10^{-4} to 10^{-5} cm, and high temperatures, do the adion concentrations approach the maximum step capacities. The fact that the kink and step adion concentrations are of comparable orders of magnitude, although the energy to bring a fluorine ion from the bulk to the kink is considerably lower than that for the adsorption at the step (see table 1), can be interpreted by two facts: first, the formation energy of the kinks (0.47 eV, compare section 3) also enters the problem; second, the probability of arranging the adions at the step is considerably larger than that at the nearly filled-up kink sites.

As an example, the dependence of the bulk concentrations of the vacancies, n_v, and interstitials, n_i, are plotted as a function of the distance from the surface in figure 7 for a temperature of 750 K with the step distance λ as a parameter. Here, again, the experimental accessible range is shaded. The bulk concentrations of both defects, which are given by

$$n_\mathrm{v}^\infty = n_\mathrm{i}^\infty = \sqrt{2} N_\mathrm{b} \exp(-F_\mathrm{f}/2kT) = 2 \times 10^{13}\ \mathrm{cm}^{-3}, \tag{15}$$

are indicated as a broken line. The extension of the space-charge layer, κ^{-1}, at this temperature amounts to about 1 μm. While with decreasing distance from the surface the vacancy concentration increases by a factor of about 450–2100 for $\lambda = 10^{-5}$–10^{-6} cm, the interstitial concentration shows a corresponding decrease, so that the product of both concentrations remains constant throughout the space-charge region. However, due to the increase of the anion vacancy concentration on approaching the surface, the sum of both charge carriers increases considerably above that in the bulk. This should cause, in addition, an increased ionic conductivity in the near-surface region of the crystal as well as in thin fluorite crystal layers [13]. The latter case will be treated in the next section in greater detail.

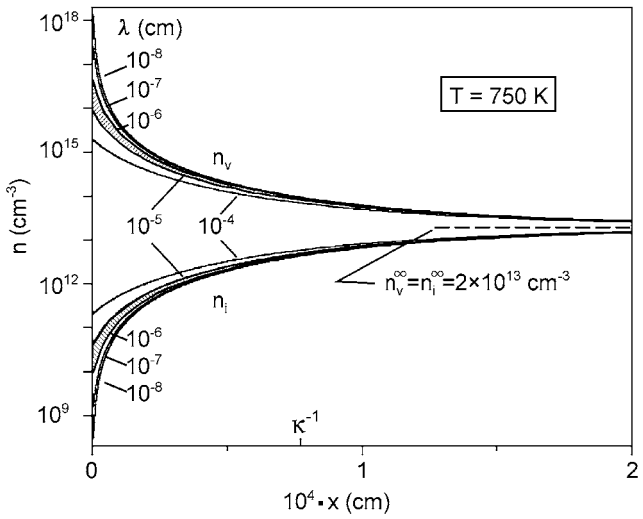

Figure 7. Concentrations of vacancies and interstitials, n_v and n_i, for a temperature of 750 K as a function of the distance from the surface. The broken curve on the right axis indicates the bulk value of both concentrations. The extension of the space-charge layer κ^{-1} at this temperature is indicated at the bottom axis,

4.2. Thin CaF_2 layer

Because of the fundamental interest in the physical and chemical properties of thin layers, among others in their electrical conductivity, compare section 1, the calculations were extended to the case of thin mono-crystalline CaF_2 layers (thickness: $2L$) with two free (111) surfaces. Results for a temperature of the CaF_2 layer of 750 K and a mean step distance $\lambda = 5 \times 10^{-6}$ cm on both surfaces are discussed in the following. (This temperature was chosen because it is close to the middle of the temperature range, for which experimental conductivity data are known, see figure 11.) Figure 8 shows a comparison of the potential Φ_L for different L (broken curve) with the near-surface course of the potential $\Phi(x)$ for a crystal with unlimited thickness (full curve). With increasing thickness of the layer Φ_L approaches the potential Φ_∞ for $x \to \infty$ indicated on the right axis. In addition, the course of the potential $\Phi(x)$ in a layer of thickness $2L = 2 \times 10^{-4}$ cm (dotted curve) is given. The largest absolute deviation of the layer potential from that of an unlimited crystal occurs at $x = L$, while with decreasing distance from the surface the layer potential adopts that of the unlimited crystal.

Figure 9 shows a corresponding comparison of the courses of the fluorine vacancy and the interstitial concentrations of the 2×10^{-4} cm thick layer with those in the near-surface region of an unlimited crystal. Also the concentrations approximate those of the unlimited crystal for decreasing distance from the surface. It may be seen from this figure that the total of the mean vacancy and interstitial concentrations in this layer is, due to the overlapping of the space-charge regions at both surfaces, larger than in the space-charge region of the semi-infinite crystal. In figure 10 the surface concentrations n_k, n_l and n_t are given as functions of the layer thickness. Since, with decreasing L, the total charge in the layer decreases, the surface charges show a corresponding decrease. Under the present conditions it is remarkable that this decrease becomes distinct at the step and terrace concentrations for L below about 1×10^{-5} cm. The kinks, in contrast, because of their low energy difference with respect to the bulk sites (compare figure 3), remain nearly saturated.

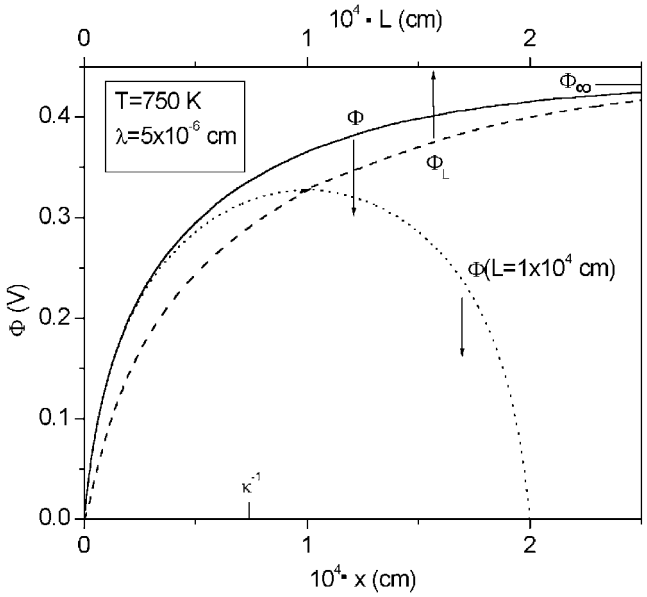

Figure 8. Comparison of the potential Φ_L of a CaF_2 layer of thickness $2L$ as a function of L (broken curve) with the potential $\Phi(x)$ for infinite thickness of the crystal (full curve) for $T = 750$ K and a mean step distance $\lambda = 5 \times 10^{-6}$ cm. As an example, the course of the potential $\Phi(x)$ for a $2L = 2 \times 10^{-4}$ cm thick layer is given (dotted curve). Φ_∞ for this temperature and step distance is indicated on the right axis.

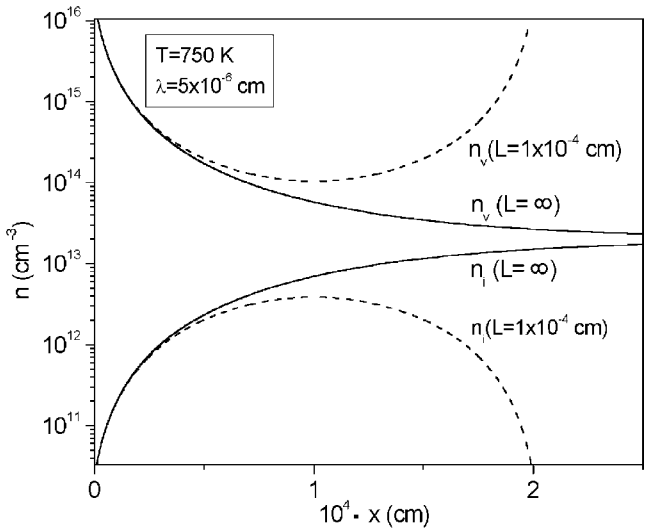

Figure 9. Comparison of the vacancy and interstitial concentrations, n_v and n_i, respectively, for a $2L = 2 \times 10^{-4}$ cm thick layer (broken curves) with the concentrations for infinite thickness (full curves), compare also figure 7, as a function of x for $T = 750$ K and $\lambda = 5 \times 10^{-6}$ cm.

The mean electrical conductivity of a thin CaF_2 layer of the half-thickness L can be calculated from the mean vacancy and interstitial concentrations, $\bar{n}_v(L)$ and $\bar{n}_i(L)$, according

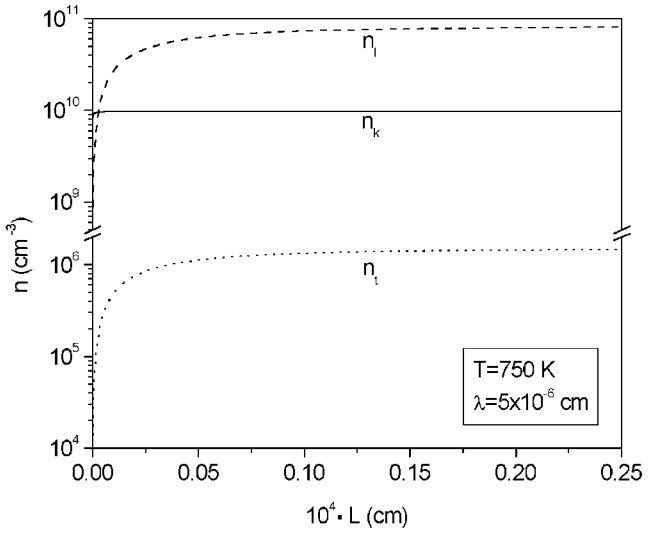

Figure 10. Dependence of the kink, step and terrace concentrations, n_k, n_l and n_t, of F_{ad}^- ions on the surface on the thickness of a $2L$ thick CaF_2 layer for $T = 750$ K and $\lambda = 5 \times 10^{-6}$ cm.

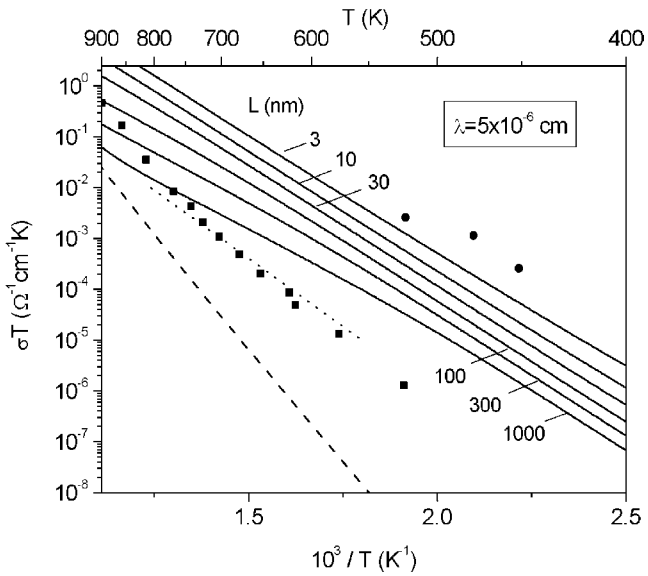

Figure 11. Mean ion conductivity, $\sigma_L T$, of thin CaF_2 layers as a function of the temperature for different half-thickness L (full lines). Broken line: bulk conductivity of CaF_2 [27]; dotted line: experimental mean conductivity of a 500 nm thick CaF_2 layer [28]; symbols: conductivity data for grained CaF_2 (squares: $r_{\text{grain}} = 0.2$ μm, circles: $r_{\text{grain}} = 9$ nm) [18].

to

$$\sigma_L = \sigma_{\text{v}}^{\infty} \frac{\bar{n}_{\text{v}}(L)}{n_{\text{v}}^{\infty}} + \sigma_{\text{i}}^{\infty} \frac{\bar{n}_{\text{i}}(L)}{n_{\text{i}}^{\infty}}, \tag{16}$$

where $\sigma_{\text{v}}^{\infty}$ and $\sigma_{\text{i}}^{\infty}$ are the conductivities and $n_{\text{v}}^{\infty} = n_{\text{i}}^{\infty}$ the concentrations of the vacancies and interstitials, respectively, in the bulk of the crystal. The product of the overall conductivity

and the temperature, $\sigma_L T$, for different half-thickness, L, of the CaF_2 layer was calculated, again for a step distance of 5×10^{-6} cm, using bulk conductivity data given by Bollmann and Reimann [27], see the full lines in figure 11. Beside the bulk conductivity (broken line) [27] this figure also includes experimental data obtained for an about 500 nm thick epitaxial CaF_2 layer on an Al_2O_3 substrate using a thin intermediate BaF_2 layer (dotted line) [28] as well as conductivity data of differently grained CaF_2, $r_{grain} = 0.2$ μm (squares) and $r_{grain} = 9$ nm (circles) [18]. The observed increase in conductivity with decreasing layer thickness and grain size, respectively, which is also found in studies with alternating CaF_2/BaF_2 layers of different thickness [28], is a clear indication of the overlapping space charges. The difference of the conductivity of the fine-grained material compared with that of the theoretical thin layer results for $\lambda = 5 \times 10^{-6}$ cm may be attributed: (i) to a different number of surface sites for the take-up of excess fluor ions, (ii) to the fact that, for a grain, which has finite extensions in three dimensions, the overlapping should be yet larger, and (iii) to an increasing part of the ionic conductivity on the surface itself. The decreasing slope of the fine-grained material at higher temperatures is attributed to grain coarsening [18]. In all, a good correspondence of our theoretical results with experimental conductivity data is achieved, which may be seen as a confirmation of our above derivations.

5. Conclusions

In the present paper the properties of the FD layer at the surface of a fluorite type crystal with anti-Frenkel disorder were examined theoretically. Numerical calculations were performed for the (111) surface of a semi-infinite pure (undoped) CaF_2 crystal as well as for thin CaF_2 layers with free (111) surfaces considering realistic step and kink concentrations. For this the determination of the adsorption positions and energies of the fluor ion at sites on the terrace and at the ledge and kink was also necessary. The calculations have shown that steps and kinks are likewise responsible for the take-up of the excess fluor ions on the surface, whereas the terrace plays no role. For experimentally accessible conditions, i.e. for step distances between 10^{-6} and 10^{-5} cm, the electrical potential between surface and bulk, and with it the variations of the anion vacancy and interstitial concentrations in the surface layer, are considerably reduced against those for an unlimited number of available surface sites. Nevertheless, also for realistic step distances due to the increased concentrations of the anion vacancies a strongly increased near-surface ionic conductivity is expected. This is of importance above all for the ionic conductivity of thin layers and nano-crystalline material, whose experimental conductivity data show a good correspondence to our results.

Epitaxial layers of CaF_2 are presently being investigated as protecting and intermediate layers on semiconductors (compare section 1). Though the specific interface will strongly influence the characteristics of the isolator layer the present calculations may serve as a first approximation and/or as a standard with which actual results may be compared. Increased ion conductivities were recently reported by Sata *et al* [28] for heterolayered films of CaF_2 and BaF_2 (see above). It is known from our own studies of heteroepitaxial systems that growth of the guest component starts usually at the steps on the substrate surface [29, 30]. This should occur also for BaF_2/CaF_2 epilayers. In this way, kink and step sites may be blocked for an incorporation of excess anions. However, the misfit of 13.5% between both lattices, which should be accommodated within the first grown layers by misfit dislocations, may serve for a sufficient number of adsorption sites at the interface. It cannot be excluded that, due to this relatively large misfit, an increased number of adsorption sites compared to that at a free surface may be present. For BaF_2/CaF_2, in addition, further effects due to the different bonding energies in normal and interstitial lattice sites in both components are expected.

Besides conductivity measurements, an experimental proof of the course of the potential in the space-charge region may be performed by studying the distribution of small amounts of an aliovalent tracer [31, 32] dissolved in the crystal. In general, the above calculations may be further extended to the extrinsic case, i.e. to a doping with aliovalent cations and also to the case of the formation of defect clusters, which will occur, above all, at lower temperatures.

Acknowledgments

This work was performed during a stay of one of the authors (MFB) at the Mineralogical Institute of the University of Bonn. This author expresses his gratitude to the Deutsche Akademische Austauschdienst (DAAD) for the financial support of this stay in Germany.

Appendix A

For the determination of the minimum of the Gibbs free energy given in equation (1) the condition of electrical neutrality is introduced in this equation by the method of the Lagrange multiplier α. The variation of

$$\delta\tilde{G} = \delta\left\{G + \alpha\left[n_\mathrm{k} + n_\mathrm{l} + n_\mathrm{t} - \int_0^\infty [n_\mathrm{v}(x) - n_\mathrm{i}(x)]\,\mathrm{d}x\right]\right\} \tag{A.1}$$

is produced by a set of independent variations δn_ν in n_ν, $\nu = \mathrm{v, i, k, l, t}$:

$$\begin{aligned}\delta\tilde{G} = \int_0^\infty \Bigg\{ & \delta n_\mathrm{i}(x)[F_\mathrm{f} + \alpha] - \delta n_\mathrm{v}(x)\alpha + \tfrac{1}{2}\delta[\rho(x)\Phi(x)] \\ & - \delta n_\mathrm{v}(x)\,kT\ln\frac{2N_\mathrm{b}}{n_\mathrm{v}(x)} - \delta n_\mathrm{i}(x)\,kT\ln\frac{N_\mathrm{b}}{n_\mathrm{i}(x)}\Bigg\}\,\mathrm{d}x \\ & + \delta n_\mathrm{k}[F_\mathrm{k} + \alpha] + \delta n_\mathrm{l}[F_\mathrm{l} + \alpha] + \delta n_\mathrm{t}[F_\mathrm{t} + \alpha] \\ & - \delta n_\mathrm{k}\,kT\ln\frac{N_\mathrm{k} - n_\mathrm{k}}{n_\mathrm{k}} - \delta n_\mathrm{l}\,kT\ln\frac{N_\mathrm{l} - n_\mathrm{l}}{n_\mathrm{l}} - \delta n_\mathrm{t}\,kT\ln\frac{N_\mathrm{t} - n_\mathrm{t}}{n_\mathrm{t}}.\end{aligned} \tag{A.2}$$

The variation of the electrostatic energy yields [3]

$$\tfrac{1}{2}\int_0^\infty \delta[\rho(x)\Phi(x)]\,\mathrm{d}x = e\int_0^\infty \Phi(x)[\delta n_\mathrm{v}(x) - \delta n_\mathrm{i}(x)]\,\mathrm{d}x. \tag{A.3}$$

In the minimum of the Gibbs free energy $\delta\tilde{G} = 0$ and the individual concentrations n_ν result as

$$\begin{aligned} n_\mathrm{v}(x) &= 2N_\mathrm{b}\exp\left(-\frac{e\Phi(x) - \alpha}{kT}\right) \\ n_\mathrm{i}(x) &= N_\mathrm{b}\exp\left(-\frac{F_\mathrm{f} - e\Phi(x) + \alpha}{kT}\right) \\ n_\mathrm{k} &= N_\mathrm{k}\left\{1 + \exp\left(\frac{F_\mathrm{k} + \alpha}{kT}\right)\right\}^{-1} \\ n_\mathrm{l} &= N_\mathrm{l}\left\{1 + \exp\left(\frac{F_\mathrm{l} + \alpha}{kT}\right)\right\}^{-1} \\ n_\mathrm{t} &= N_\mathrm{t}\left\{1 + \exp\left(\frac{F_\mathrm{t} + \alpha}{kT}\right)\right\}^{-1}. \end{aligned} \tag{A.4}$$

Whereas here bulk vacancy and interstitial concentrations are assumed to be small against the density of total bulk sites, i.e. $n_\mathrm{v},\ n_\mathrm{i} \ll N_\mathrm{b}$, the formulation for n_k, n_l, and n_t considers the fact

that these concentrations may be of the same order of magnitude as the total numbers of kink, step and terrace sites, N_k, N_l and N_t, respectively. In the bulk (for large x) the space-charge vanishes, i.e.

$$\rho_\infty = 0, \tag{A.5}$$

which corresponds to

$$n_v^\infty = n_i^\infty \tag{A.6}$$

or, according to equation (A.4), to

$$2\exp\left(-\frac{e\Phi_\infty - \alpha}{kT}\right) = \exp\left(-\frac{F_f - e\Phi_\infty + \alpha}{kT}\right), \tag{A.7}$$

where $\Phi_\infty = \Phi(x = \infty)$. Defining

$$F_v = -kT \ln 2 \tag{A.8}$$

it follows from equation (A.7) that

$$\exp\left(-\frac{F_v + e\Phi_\infty - \alpha}{kT}\right) = \exp\left(-\frac{F_f - e\Phi_\infty + \alpha}{kT}\right). \tag{A.9}$$

The Lagrange multiplier results then as

$$\alpha = \frac{F_v - F_f}{2} + e\Phi_\infty. \tag{A.10}$$

Replacing α in equations (A.4) Poisson's equation (5) can be rewritten as

$$\frac{d^2}{dx^2}\left\{\frac{e\Phi(x) - e\Phi_\infty}{kT}\right\} = \frac{4\pi e^2 N_b}{\epsilon kT}\exp\left(-\frac{F_v + F_f}{2kT}\right) \times \left\{\exp\left(\frac{e\Phi(x) - e\Phi_\infty}{kT}\right) - \exp\left(-\frac{e\Phi(x) - e\Phi_\infty}{kT}\right)\right\}. \tag{A.11}$$

The solution of this second-order linear differential equation for $\Phi(x)$ proceeds by analogy to previous analyses (see, e.g., [3]). With the abbreviations

$$z(x) = \{e\Phi(x) - e\Phi_\infty\}/kT, \tag{A.12}$$

$$s = \kappa x, \tag{A.13}$$

$$\kappa^2 = \frac{8\sqrt{2}\pi e^2 N_b}{\epsilon kT}\exp\left(-\frac{F_f}{2kT}\right), \tag{A.14}$$

where the Debye length κ^{-1} gives the extension of the near-surface region, in which the potential and the defect concentrations deviate from the bulk values, one can write equation (A.11) as

$$d^2z/ds^2 = \sinh z. \tag{A.15}$$

With the boundary condition

$$dz/ds|_\infty = 0, \qquad \text{corresponding to } d\Phi(x)/dx|_\infty = 0, \tag{A.16}$$

the first integration of (A.15) results as

$$ds = -\frac{dz}{\sqrt{2}(\cosh z - 1)^{1/2}} \tag{A.17}$$

and the final solution as

$$\ln\left\{\frac{\exp(-z/2) + 1}{\exp(-z/2) - 1}\right\} = s + \ln\left\{\frac{\exp(-z_0/2) + 1}{\exp(-z_0/2) - 1}\right\}, \tag{A.18}$$

where $z_0 = -(e\Phi_\infty/kT)$. Here, without loss of generality, the potential at the surface is set as $\Phi(0) = 0$. This equation can be solved to z:

$$z = 4\tanh^{-1}\{\exp(-s)\tanh(z_0/4)\} \tag{A.19}$$

with

$$\tanh^{-1}(\xi) = \frac{1}{2}\ln\left(\frac{1+\xi}{1-\xi}\right) \qquad \text{for } -1 < \xi < 1. \tag{A.20}$$

The potential Φ_∞ between surface and bulk is connected with the actual surface charge. For the determination of Φ_∞ we start from the correspondence between surface charge and potential gradient at the surface:

$$\sigma = -\frac{\epsilon}{4\pi}\left.\frac{\mathrm{d}\Phi}{\mathrm{d}x}\right|_{x=0}. \tag{A.21}$$

From equation (A.17) using (A.12) the gradient of the potential at the surface is obtained as

$$\left.\frac{\mathrm{d}\Phi}{\mathrm{d}x}\right|_{x=0} = -\frac{\sqrt{2}\kappa kT}{e}\left\{\cosh\left(-\frac{e\Phi_\infty}{kT}\right) - 1\right\}^{1/2}, \tag{A.22}$$

from which the surface charge

$$\sigma = \frac{\epsilon\kappa kT}{2\pi e}\sinh\left(-\frac{e\Phi_\infty}{2kT}\right) \tag{A.23}$$

results. From this equation with (3) and (7) after replacing F_v, α, and κ according to equations (A.8), (A.10) and (A.14), equation (6) for Φ_∞ is obtained.

Appendix B

In the case of a thin layer of extension $2L$ with the boundary equation

$$\mathrm{d}z/\mathrm{d}s|_L = 0, \tag{B.1}$$

compare equation (8), a first integration of the normalized Poisson equation (A.15) yields

$$\mathrm{d}s = -\frac{1}{\sqrt{2}}\frac{\mathrm{d}z}{(\cosh z - \cosh z_L)^{1/2}}, \tag{B.2}$$

from which the solution of (A.15) results as [3]

$$s = \tilde{k}F\left(\sin^{-1}\left\{\frac{\cosh z_0 - \cosh z_L}{\cosh z_0 - 1}\right\}^{1/2}, \tilde{k}\right) - \tilde{k}F\left(\sin^{-1}\left\{\frac{\cosh z(s) - \cosh z_L}{\cosh z(s) - 1}\right\}^{1/2}, \tilde{k}\right), \tag{B.3}$$

where $F(\phi, \tilde{k})$ is the incomplete elliptic integral of the first kind, ϕ being the first argument in the parentheses, and with

$$\tilde{k} = \left(\frac{2}{\cosh z_L + 1}\right)^{1/2}, \tag{B.4}$$

$$z_0 = z|_{s=0} = -e\tilde{\Phi}_\infty/kT, \tag{B.5}$$

and

$$z_L = \kappa L = \{e\Phi_L - e\tilde{\Phi}_\infty\}/kT, \tag{B.6}$$

where Φ_L denotes the potential at $x = L$. Here, $\tilde{\Phi}_\infty$ is rather a parameter corresponding to the Lagrange multiplier α. It takes values, which are larger than the potential difference between

surface and bulk in the semi-infinite case, see section 2.1. However, for increasing layer width, $\tilde{\Phi}_\infty$ and Φ_L approximate to the semi-infinite value Φ_∞.

Because of the complexity of the interdependence of the different parameters encountered in this problem our practical proceeding for the evaluation shall be shortly outlined. Choosing an arbitrary value for $\tilde{\Phi}_\infty \geqslant \Phi_\infty$ with equation (9) a corresponding value of Φ_L is calculated. With these values, instead of using the solution (B.3), we perform a complete integration of equation (B.2), which leads for the left-hand side to s. Numerical integration of the right-hand side with respect to z yields $z(s)$ and $\Phi(x)$, respectively. For an integration up to an upper limit of z_L this integral also determines the value of L belonging to the chosen parameter $\tilde{\Phi}_\infty$.

References

[1] Frenkel J 1946 *Kinetic Theory of Liquids* (New York: Oxford University Press) p 36
[2] Lehovec K 1953 *J. Chem. Phys.* **21** 1123
[3] Kliewer K L and Koehler J S 1965 *Phys. Rev.* A **140** 1226
[4] Blakely J M and Danyluk S 1973 *Surf. Sci.* **40** 37
[5] Margvelashvili I G and Saralidze Z K 1980 *Sov. Phys.—Solid State* **22** 868
[6] Kliewer K L 1966 *J. Phys. Chem. Solids* **27** 705
[7] Eshelby J, Newey C, Pratt P and Lidiard A 1958 *Phil. Mag.* **3** 75
[8] Poeppel R B and Blakely J M 1969 *Surf. Sci.* **15** 507
[9] Engelhardt B J, Dabringhaus H and Wandelt K 2000 *Surf. Sci.* **448** 187
[10] Deuster V, Schick M, Kayser Th, Dabringhaus H, Klapper H and Wandelt K 2003 *J. Cryst. Growth* **250** 313
[11] Schick M, Dabringhaus H and Wandelt K 2003 in preparation
[12] Liberman V, Bloomstein T M, Rothschild M, Sedlacek J H C, Uttaro R S, Bates A K, Van Peski C and Orvek K 1999 *J. Vac. Sci. Technol.* B **17** 3273
[13] Liu W K, Fang X M, Winesett J, Ma W, Zhang M B, Santos M B and McCann P J 1997 *J. Cryst. Growth* **175/176** 853
[14] Schroeder B R, Meng S, Bostwick A, Olmstead M A and Rotenberg E 2000 *Appl. Phys. Lett.* **77** 1289
[15] Dabringhaus H and Wandelt K 2003 *Surf. Sci.* **526** 257
[16] Dabringhaus H and Wandelt K 2003 *Surf. Sci.* **526** 273
[17] Lidiard A B 1974 *Crystals with the Fluorite Structure* ed W Hayes (Oxford: Claredon) p 101
[18] Maier J 2000 *Solid State Ion.* **131** 13
[19] National Bureau of Standards (US) 1984 *Monograph 25* **21** 52
[20] Dabringhaus H 2000 *Surf. Sci.* **462** 123
[21] Catlow C R A, Norgett M J and Ross T A 1977 *J. Phys. C: Solid State Phys.* **10** 1627
[22] Dornford-Smith A and Grimes R W 1995 *Phil. Mag.* B **72** 563
[23] Dick B G and Overhauser A M 1958 *Phys. Rev.* **112** 90
[24] Heyes D M, Barber M and Clark J H R 1977 *J. Chem. Soc. Faraday Trans.* **75** 485
[25] Gay D H and Rohl A L 1995 *J. Chem. Soc. Faraday Trans.* **91** 925
[26] Keller G W 1964 *Handbook of Physical Constants* ed S P Clark (New York: Geological Society of America) p 565
[27] Bollmann W and Reimann R 1973 *Phys. Status Solidi* a **16** 187
[28] Sata H, Eberman K, Eberl K and Maier J 2000 *Nature* **408** 946
[29] Haag M and Dabringhaus H 1997 *J. Cryst. Growth* **178** 287
[30] Klumpp St and Dabringhaus H 1999 *J. Cryst. Growth* **204** 487
[31] Hudson R A, Farlow G C and Slifkin L M 1987 *Phys. Rev.* B **36** 4651
[32] Wonell S K and Slifkin L M 1993 *Phys. Rev.* B **48** 78